

Experimental Comparison of Two Quantum Computing Architectures

N. M. Linke^{a,1}, D. Maslov^b, M. Roetteler^c, S. Debnath^a, C. Figgatt^a, K. A. Landsman^a, K. Wright^a, and C. Monroe^{a,d}

^aJoint Quantum Institute, Department of Physics, and Joint Center for Quantum Information and Computer Science, University of Maryland, College Park, MD 20742, USA; ^bNational Science Foundation, Arlington, VA 22230, USA; ^cMicrosoft Research, Redmond, WA 98052, USA; ^dIonQ Inc., College Park, MD 20742, USA

This manuscript was compiled on October 30, 2016

We run a selection of algorithms on two state-of-the-art 5-qubit quantum computers that are based on different technology platforms. One is a publicly accessible superconducting transmon device [1] with limited connectivity, and the other is a fully connected trapped-ion system [2]. Both can be programmed in a way that is blind to the underlying hardware. We show that algorithms requiring more interconnections demonstrate the advantage of using a highly connected system, implying the need for co-designing quantum applications with hardware.

Quantum Computing | Quantum Information Science

Inspired by the vast computing power a universal quantum computer could offer, several candidate systems are being explored. They have allowed experimental demonstrations of quantum gates, operations, and algorithms of ever-increasing sophistication. Recently, two architectures, superconducting transmon qubits [3–6] and trapped ions [2, 7], have reached a new level of maturity. They have become fully programmable multi-qubit machines that provide the user with the flexibility to implement arbitrary quantum circuits from a high-level interface. This makes it possible for the first time to test quantum computers irrespective of their particular physical implementation.

While the quantum computers considered here are still small-scale and their capabilities do not currently reach beyond small demonstration algorithms, this line of inquiry can still provide useful insights into the performance of existing systems and the role of architecture in quantum computer design. These will be crucial for the realization of more advanced future incarnations of the present technologies.

The standard abstract model of quantum computation assumes that interactions between arbitrary pairs of qubits are available. However, physical architectures will in general have certain constraints on qubit connectivity. These restrictions do not in principle limit the ability to perform arbitrary computations, since SWAP operations may be used to effect gates between arbitrary qubits using the connections available. The increase in circuit cost will depend on the type of graph the system represents. For a general circuit, going from the optimal (fully connected) to the worst case (star-shaped or linear nearest-neighbor) connectivity requires an increase in the number of gates of $O(n)$, where n is the number of qubits [8]. How much overhead is incurred in practice depends on the connections used in a particular circuit and how efficiently they can be matched to the physical qubit-to-qubit interaction graph.

In this article, we make use of the public access recently granted by IBM to a 5-qubit superconducting device (illustrated in fig.1(a)) via their “Quantum Experience” cloud service [1]. This allows us to repeat algorithms that we perform

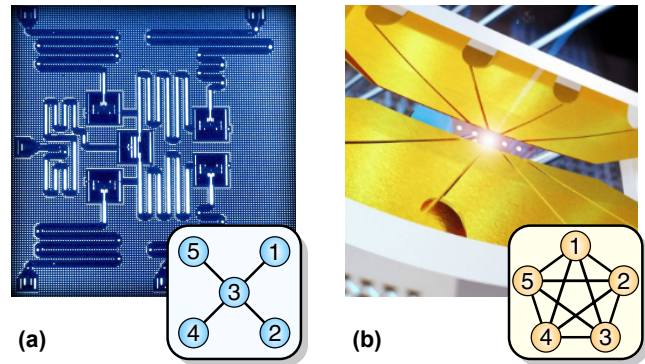


Fig. 1. Graphic representations of the two systems: (a) the superconducting qubits connected by microwave resonators (Credit: IBM Research), and (b) the linear chain of trapped ions connected by laser-mediated interactions. Insets: Qubit connectivity graphs, star-shaped (a) and fully connected (b).

in our own ion trap experiment on an independent quantum computer of identical size and comparable capability but with a different physical implementation at its core.

Physical Hardware

The ion trap system consists of five $^{171}\text{Yb}^+$ ions which are confined in a linear Paul trap and laser-cooled close to their motional ground state (see fig.1(b)) [2]. The qubits are magnetic-field-insensitive pairs of states in the hyperfine-split $^2S_{1/2}$ ground-level of each atom, which gives a qubit frequency of

Significance Statement

Quantum computers are an emerging technology promising to be vastly more powerful at solving certain problems than any conventional computer. These devices are now moving out of the laboratory and becoming generally programmable. This allows identical quantum tasks or algorithms to be implemented on radically different technologies to inform further development and scaling. We run a series of algorithms on the two leading platforms: trapped atomic ions and superconducting circuits. While the superconducting system offers faster gate clock speeds and a solid-state platform, the ion trap system features superior qubits and reconfigurable connections. The performance of these systems is seen to reflect the level of connectivity in the base hardware, indicating that quantum computer applications and hardware should be “co-designed”.

C. Monroe is the co-founder and Chief Technical Officer of IonQ, Inc.

¹To whom correspondence should be addressed. E-mail: linke@umd.edu

Table 1. Single- and two-qubit gate counts for the circuits on the superconducting (star-shaped) and the ion trap (fully connected) system after mapping to the respective hardware using the respective gate libraries. For comparison, the gate counts for a linear nearest-neighbor (LNN) architecture as implemented in [3] are included. We also note the gate count for the Quantum Fourier Transform (QFT) for 3 and 5 qubits. The latter was implemented in [2] using a sequence of modular gates that was not optimized for gate count. The QFT-5 cannot be implemented exactly using the current IBM gate library. If we assume Z^a operations are possible, the counts shown as * are 47 for single- and 29 for two-qubit gates.

connectivity	star-shaped		LNN		fully conn.	
hardware	supercond.				ion trap	
gate library	Clifford+T		Clifford+ Z^a		R/XX	
gate type	single	two	single	two	single	two
Margolus	20	3	20	3	11	3
Toffoli	17	10	9	10	9	5
Bernstein-Vazirani	10	0-4	10	0-10	14-26	0-4
Hidden Shift	28-34	10	20-26	4	42-50	4
QFT-3	42	19	11	7	8	3
QFT-5	*	*	35	28	22	10

Algorithms

Margolus and Toffoli Gate. The Toffoli gate is a 3-qubit controlled-controlled-NOT gate that requires 6 CNOT gates [26, 27]. It is possible to implement a Toffoli with 5 entangling gates if the square-root of the CNOT operation is available [15], which is the case with the trapped ion XX gate. The Margolus gate is a simplified version of the Toffoli operation, which introduces an additional phase on the state corresponding to $|100\rangle$. It can be realized with just 3 CNOT gates [28, 29]. The circuits are shown in figure 2(a,b). Note that for the Margolus gate, all entangling operations connect to the same qubit, which means that this circuit can be realized efficiently with star-shaped qubit connectivity. The systems perform this circuit at success probability 74.1(7)% for superconductors and 90.1(2)% for ions (see figure 3(a1,b1)).

The full Toffoli circuit uses the same three qubits as the Margolus implementation so that preparation and measurement errors remain the same. The optimized circuit for the fully connected ion trap system contains 5 two-qubit gates and the additional operations lower the fidelity to 85.0(2)% (see figure 3(b2)). For the star-shaped system, an additional 7 two-qubit gates are needed to effect the SWAP operations necessary to go from the Margolus to the full Toffoli gate. This leads to a reduced success rate of 52.6(8)% for the superconducting system (3(a2)). Note that the transformation $|a, b, c\rangle \rightarrow |c \oplus ab, b, a\rangle$ may be obtained with the Clifford+T library on a star-shaped graph with the provably minimal number of 7 CNOT gates. We do not consider such input-to-output mappings of the composite gates in this work. However, we always choose the most favorable input-to-output mapping for the IBM star and LNN architectures when executing entire quantum algorithms, which is merely a classical swap between physically measured signals.

Bernstein-Vazirani and Hidden Shift Algorithms. In the Bernstein-Vazirani algorithm, an oracle implements the function $f_c(\mathbf{x}) = \mathbf{x} \cdot \mathbf{c}$. The algorithm finds the unknown bit string \mathbf{c} in a single shot. In the oracle, \mathbf{c} is encoded in a pattern of CNOT gates, all of which target the ancilla qubit [30]. As can be seen from the circuit in figure 2(c), the entire algorithm maps well onto

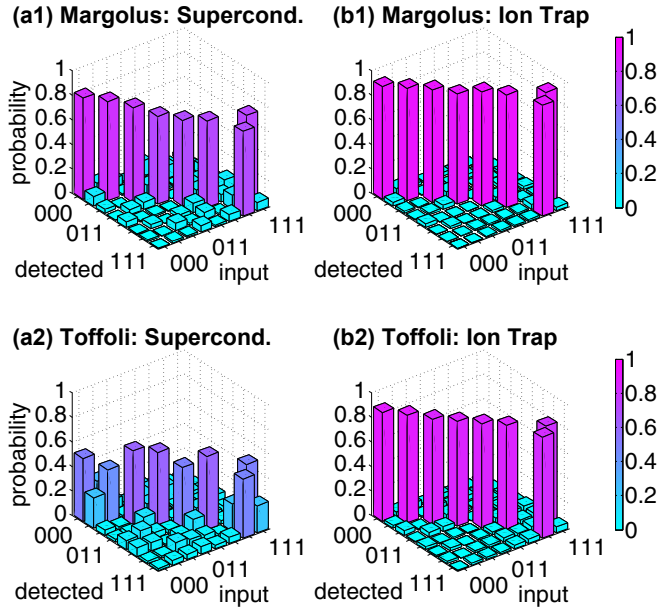


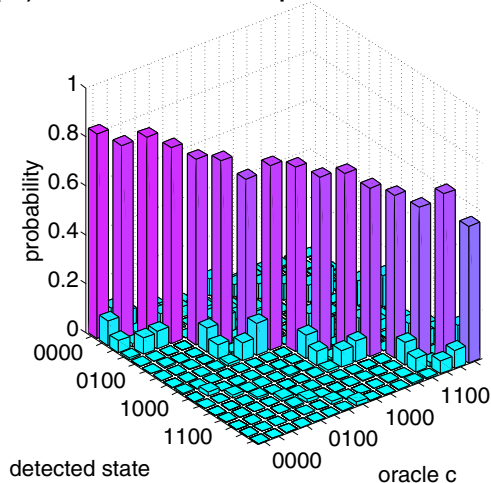
Fig. 3. Margolus gate results from the star-shaped superconductor (a1) and the fully connected ion trap system (b1). The fidelities are 74.1(7)% and 90.1(2)%, respectively. The full Toffoli gate results give success probabilities of 52.6(8)% for the superconducting (a2) and 85.0(2)% for the ion trap (b2) system. The axes represent states as 3-bit binary numbers. For each input state, the probabilities of detecting each state are shown.

a star-shaped architecture. This algorithm is very similar to a parity check circuit used in error correction applications, and indeed the IBM system was laid out with this application in mind [6]. The single-shot success probabilities are 72.8(5)% for the star-shaped superconducting system and 85.1(1)% for the fully connected ion trap system (figure 4(a1,b1)).

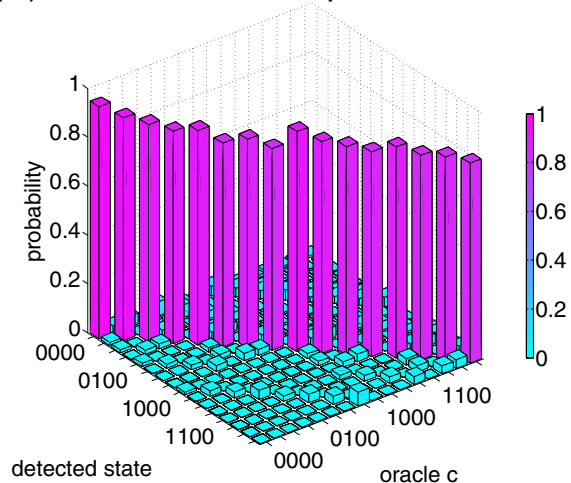
To compare this to a similar algorithm with different connectivity requirements, we implement the hidden shift algorithm [31] for a black box bent function [32, 33]. An oracle implements the shifted version $f(\mathbf{x}+\mathbf{s})$ of the known Boolean function f . We want to determine the n -bit string \mathbf{s} that constitutes the “hidden shift”. For a subset of Boolean functions, there exists a quantum algorithm that can solve this problem in a single oracle query, while classical algorithms require $\Omega(\sqrt{2^n})$ queries. This subset contains functions which have a flat Fourier spectrum and whose dual f^\sim can be calculated efficiently, i.e. so-called bent functions of the Maierana-McFarland class [33]. Here we choose the 4-bit function $f(\mathbf{x}) = x_1x_2 \oplus x_3x_4$ for which $f = f^\sim$. We implement all possible 4-bit shift patterns \mathbf{s} using the circuit shown in figure 2(d). The algorithm output state directly corresponds to the hidden shift \mathbf{s} . The circuit involves gates between two disconnected pairs of qubits, which creates an overhead of 6 two-qubit gates for a star-shaped architecture. The results are shown in figure 4(a2,b2). The fidelity of the fully connected ion trap implementation is 77.1(2)% compared to 35.1(6)% for the superconducting device. The numerical values of the data plotted in figure 3 and 4 are reproduced as tables in the Appendix.

The errors in both devices appear concentrated in certain sets of states, leading to patterns in the off-diagonal elements of the result plots (see figure 4). These highly structured signatures suggest that systematic errors dominate, especially

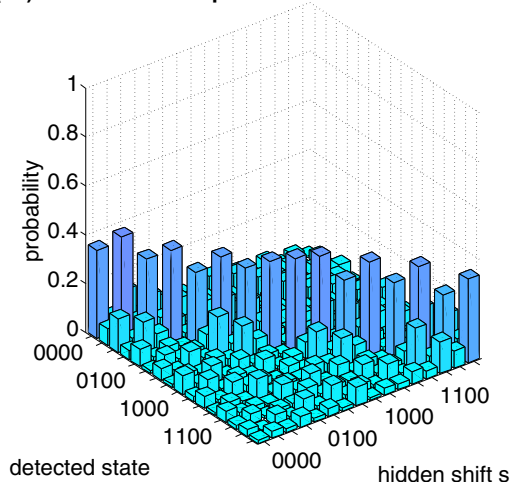
(a1) Bernstein-Vazirani: Superconductor



(b1) Bernstein-Vazirani: Ion Trap



(a2) Hidden shift: Superconductor



(b2) Hidden shift: Ion Trap

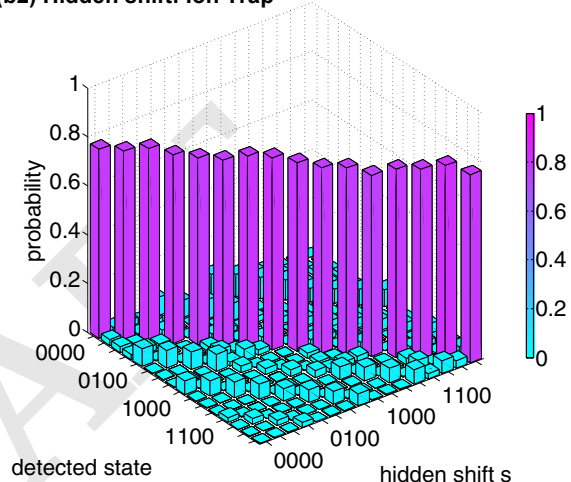


Fig. 4. Results from the Bernstein-Vazirani algorithm implementing the oracle function $f_c(\mathbf{x}) = x_0c_0 \oplus c_1x_1 \oplus c_2x_2 \oplus c_3x_3$ for all possible 4-bit oracles \mathbf{c} performed on the star-shaped (a1) and the fully connected (b1) systems. The average success probabilities are 72.8(5)% for the superconductor and 85.1(1)% for the ion trap system. Hidden shift algorithm for $f(\mathbf{x}) = x_0x_1 \oplus x_2x_3$. All possible 4-bit shifted oracle functions are implemented on the superconducting system (a2) as well as the ion trap (b2). The average success probabilities are 35.1(6)% and 77.1(2)%, respectively. The axes represent states and oracle parameters as 4-bit binary numbers.

readout errors. The grouped patterns such as in figure 4(a1) indicate flips of the least-significant bits, while parallel lines correspond to the most significant bits changing their state. In the trapped ion results, these lines can be modulated in height due to read-out crosstalk and are more pronounced on the lower-numbered state side due to $1 \rightarrow 0$ being the dominant detection error channel. Finally, we stress that comparing quantum computations across systems depends on the specifics of errors propagation, which will vary between different hardware, through their particular connectivity and physical errors. We summarize the success probabilities for the implemented circuits on both machines in Table 2. We also show the expected values for two simple error propagation models based on the error ϵ_g of individual gates and ϵ_M of M -qubit single shot readout for both systems. The first model assumes random error propagation per operation with overall error $(1 - \epsilon_M)^M (1 - \epsilon_g)^{\sqrt{N}}$ while the second is based on systematic (coherent) over- or under-rotations with overall error $(1 - \epsilon_M)^M (1 - \epsilon_g)^N$ where N is the number of gates. We see that the numbers are broadly consistent, with

random errors better predicting the superconducting system while the ion trap performance falls in between the two. The superconducting Hidden Shift algorithm is the only example with a significantly lower experimental result, perhaps from inhomogeneous errors in the device.

Outlook

All quantum computing physical platforms possess a certain level of connectivity given by their native qubit interactions and graph dimensionality. We show that qubit connectivity plays a role in quantum computing performance, by implementing the same quantum algorithms on two different platforms: a fully connected trapped ion system and a star-shaped superconducting circuit. We also see that the qubit connectivity graph is best co-designed to mirror the structure of the particular quantum circuit and that the choice of a more expressive gate library affects the efficiency of the computations. Finally, while the clock speed per quantum gate operation varies widely between these two systems, the overall speed of a quantum circuit will depend on connectivity, especially as the system is

Table 2. Summary of the achieved success probabilities for the implemented circuits, in percent. The observed probabilities (“obs”) are tabulated along side two simple error propagation models given the gate number N and the individual gate and readout errors of the two systems encapsulated in the parameters ϵ_g and ϵ_M , respectively (see main text). The first estimate assumes random (“rand”) error propagation with overall error $(1 - \epsilon_g)^{\sqrt{N}}$ while the second is based on systematic (“sys”) coherent over- or under-rotations with overall error $(1 - \epsilon_g)^N$, where N is the number of gates. The readout error for M qubits is $(1 - \epsilon_M)^M$ in both cases.

connectivity	star-shaped			fully conn.		
	supercond.			ion trap		
hardware	obs	rand	sys	obs	rand	sys
Margolus	74.1(7)	82	75	90.1(2)	91	81
Toffoli	52.6(8)	78	59	85.0(2)	89	78
Bernstein-Vazirani	72.8(5)	80	74	85.1(1)	90	77
Hidden Shift	35.1(6)	75	52	77.1(2)	86	57

scaled up.

While the results presented here see the trapped ion system achieve higher fidelities, this is a snapshot of the performance of two devices at this point in time. They are the most advanced and versatile quantum computing systems built to date but both technologies are advancing rapidly. The fully connected nature of the ion trap architecture may not scale to arbitrarily large numbers of qubits. However, full connectivity between 20 – 100 trapped ion qubits appears possible [2] and a modular approach for scaling to much larger systems with high connectivity and distance-independent operations seems promising [34, 35]. While superconducting qubits typically have limited connectivity, the automated calibration procedure and powerful user interface in the device used here accompanies a higher level of integration. Such systems-level attributes will become even more important as quantum circuits grow in complexity, regardless of physical platform.

ACKNOWLEDGMENTS. We thank D. L. Moehring, J. Kim, and K. R. Brown for key discussions, and J. Gambetta and J. Chow at IBM for their assistance in interfacing with the IBM Quantum Experience project. This work was supported by the ARO with funds from the IARPA LogiQ program, the AFOSR MURI program, and the NSF Physics Frontier Center at JQI. DM acknowledges support by the NSF. Any opinion, finding, and conclusions or recommendations expressed in this material are those of the authors and do not necessarily reflect the views of the NSF, IBM, or any of their employees.

- IBM Quantum Experience, <http://www.research.ibm.com/quantum>.
- Debnath S et al. (2016) Demonstration of a small programmable quantum computer module using atomic qubits. *Nature* 536:63–66.
- Barends R et al. (2014) Superconducting quantum circuits at the surface code threshold for fault tolerance. *Nature* 508:500–503.
- Córcoles AD et al. (2015) Demonstration of a quantum error detection code using a square lattice of four superconducting qubits. *Nature Comm.* 6:7979.
- Ofek N et al. (2016) Extending the lifetime of a quantum bit with error correction in superconducting circuits. *Nature*.
- Takita M et al. (2016) Demonstration of weight-four parity measurements in the surface code architecture. *arXiv:1605.01351v2*.
- Monz T et al. (2016) Realization of a scalable shor algorithm. *Science* 351(6277):1068–1070.
- Cheung D, Maslov D, Severini S (2007) Translation techniques between quantum circuit architectures in *Workshop on Quantum Information Processing*.
- Olmshenk S et al. (2007) Manipulation and detection of a trapped y_b^+ hyperfine qubit. *Phys. Rev. A* 76:052314.
- Mølmer K, Sørensen A (1999) Multiparticle entanglement of hot trapped ions. *Phys. Rev. Lett.* 82:1835–1838.
- Solano E, de Matos Filho RL, Zagury N (1999) Deterministic bell states and measurement of the mixed state of two trapped ions. *Phys. Rev. A* 59:R2539–R2543.
- Milburn G, Schneider S, James D (2000) Ion trap quantum computing with warm ions. *Fortschritte der Physik* 48(9-11):801–810.

- Zhu SL, Monroe C, Duan LM (2006) Trapped ion quantum computation with transverse phonon modes. *Phys. Rev. Lett.* 97:050505.
- Choi T et al. (2014) Optimal quantum control of multimode couplings between trapped ion qubits for scalable entanglement. *Phys. Rev. Lett.* 112:190502.
- Nielsen MA, Chuang IL (2011) *Quantum Computation and Quantum Information: 10th Anniversary Edition*. (Cambridge University Press, New York, NY, USA), 10th edition.
- Devoret MH, Schoelkopf PJ (2013) Superconducting circuits for quantum information: An outlook. *Science* 339(6124):1169–1174.
- Koch J et al. (2007) Charge-insensitive qubit design derived from the cooper pair box. *Phys. Rev. A* 76:042319.
- Geerlings K et al. (2013) Demonstrating a driven reset protocol for a superconducting qubit. *Phys. Rev. Lett.* 110:120501.
- Chow JM et al. (2010) Optimized driving of superconducting artificial atoms for improved single-qubit gates. *Phys. Rev. A* 82:040305.
- Chow JM et al. (2011) Simple all-microwave entangling gate for fixed-frequency superconducting qubits. *Phys. Rev. Lett.* 107:080502.
- J. Gambetta and J. Chow (2016), private communication.
- Riste D et al. (2015) Detecting bit-flip errors in a logical qubit using stabilizer measurements. *Nature Comm.* 6(6983).
- Maslov D (2016) Basic circuit compilation techniques for an ion-trap quantum machine. *arXiv:1603.07678v3*.
- Amy M, Maslov D, Mosca M, Roetteler M (2013) A meet-in-the-middle algorithm for fast synthesis of depth-optimal quantum circuits. *IEEE Transactions on Computer-Aided Design of Integrated Circuits and Systems* 32:818 – 830.
- Zajac DM, Hazard TM, Mi X, Nielsen E, R. PJ (2016) Scalable gate architecture for densely packed semiconductor spin qubits. *arXiv:1607.07025*.
- Barenco A et al. (1995) Elementary gates for quantum computation. *Phys. Rev. A* 52:3457–3467.
- Shende VV, Markov IL (2009) On the cnot-cost of toffoli gates. *Quantum Info. Comput.* 9(5):461–486.
- DiVincenzo DP (1998) Quantum gates and circuits. *Proceedings: Mathematical, Physical and Engineering Sciences* 454(1969):261–276.
- Song G, Klappenecker A (2004) Optimal realizations of simplified toffoli gates. *Quantum Info. Comput.* 4(5):361–372.
- Bernstein E, Vazirani U (1997) Quantum complexity theory. *SIAM J. Comput.* 26:1411–1473.
- van Dam W, Hallgreen S, Lawrence I (2006) Quantum algorithms for some hidden shift problems. *SIAM J. Comput.* 36(3):763–778.
- Childs A, Kothari R, Ozols M, Roetteler M (2013) Easy and Hard Functions for the Boolean Hidden Shift Problem in *Proc. TQC 2013, Leibniz International Proceedings in Informatics (LIPIcs)*. (Schloss Dagstuhl–Leibniz-Zentrum fuer Informatik), Vol. 22, pp. 50–79.
- Roetteler M (2010) Quantum algorithms for highly non-linear boolean functions in *Proceedings of the 21st Annual ACM-SIAM Symposium on Discrete Algorithms (SODA’10)*. pp. 448–457.
- Monroe C et al. (2014) Large-scale modular quantum-computer architecture with atomic memory and photonic interconnects. *Phys. Rev. A* 89:022317.
- Kielinski D, Monroe C, Wineland DJ (2002) Architecture for a large-scale ion-trap quantum computer. *Nature* 417:709–711.

Appendix

The detailed results from the algorithms presented in figures 3 and 4 are shown below as tables containing numeric probabilities. The target populations, with nominal unit probabilities, are highlighted in yellow. The others, representing errors, show a bar graph scaled from 0 to 0.1 to emphasize the systematic error patterns (see main text).

Margolus Superconductor		input state							
		000	001	010	011	100	101	110	111
detected state	000	0.8252	0.0859	0.0713	0.0107	0.1230	0.0186	0.0059	0.0293
	001	0.0791	0.8086	0.0146	0.0801	0.0156	0.1006	0.0254	0.0029
	010	0.0322	0.0039	0.7725	0.0947	0.0156	0.0078	0.0215	0.0771
	011	0.0029	0.0420	0.0576	0.7148	0.0010	0.0205	0.0752	0.0225
	100	0.0459	0.0088	0.0127	0.0039	0.6953	0.0850	0.0117	0.0771
	101	0.0039	0.0352	0.0020	0.0254	0.0762	0.7031	0.0605	0.0039
	110	0.0098	0.0020	0.0576	0.0176	0.0605	0.0088	0.1113	0.7197
	111	0.0010	0.0137	0.0117	0.0527	0.0127	0.0557	0.6885	0.0674

Margolus Ion Trap		input state							
		000	001	010	011	100	101	110	111
detected state	000	0.9180	0.0406	0.0219	0.0110	0.0292	0.0018	0.0010	0.0010
	001	0.0318	0.9156	0.0067	0.0245	0.0016	0.0288	0.0000	0.0012
	010	0.0146	0.0052	0.9151	0.0421	0.0004	0.0012	0.0124	0.0192
	011	0.0066	0.0150	0.0333	0.8954	0.0002	0.0016	0.0228	0.0112
	100	0.0278	0.0014	0.0007	0.0009	0.9274	0.0274	0.0090	0.0218
	101	0.0006	0.0210	0.0004	0.0009	0.0192	0.9158	0.0166	0.0124
	110	0.0006	0.0006	0.0120	0.0119	0.0114	0.0098	0.0376	0.9050
	111	0.0000	0.0006	0.0099	0.0134	0.0106	0.0136	0.9006	0.0282

Toffoli Superconductor		input state							
		000	001	010	011	100	101	110	111
detected state	000	0.5107	0.2832	0.0830	0.0215	0.1172	0.0693	0.0430	0.0381
	001	0.2490	0.4316	0.0156	0.0635	0.1475	0.1182	0.0322	0.0352
	010	0.0420	0.0264	0.5996	0.1250	0.0127	0.0146	0.0889	0.0654
	011	0.0234	0.0303	0.1162	0.5996	0.0205	0.0205	0.0762	0.0732
	100	0.0723	0.1084	0.0469	0.0264	0.4912	0.1152	0.0303	0.0381
	101	0.0693	0.0674	0.0156	0.0420	0.1260	0.5947	0.0283	0.0322
	110	0.0176	0.0166	0.0820	0.0625	0.0537	0.0176	0.2197	0.4990
	111	0.0156	0.0361	0.0410	0.0596	0.0313	0.0498	0.4814	0.2188

Toffoli Ion Trap		input state							
		000	001	010	011	100	101	110	111
detected state	000	0.8878	0.0298	0.0497	0.0111	0.0395	0.0089	0.0035	0.0110
	001	0.0224	0.8762	0.0101	0.0525	0.0091	0.0358	0.0133	0.0029
	010	0.0370	0.0090	0.8571	0.0385	0.0152	0.0014	0.0265	0.0224
	011	0.0075	0.0373	0.0374	0.8521	0.0015	0.0149	0.0206	0.0259
	100	0.0210	0.0082	0.0117	0.0019	0.8486	0.0332	0.0420	0.0436
	101	0.0083	0.0229	0.0017	0.0126	0.0237	0.8460	0.0350	0.0374
	110	0.0149	0.0008	0.0154	0.0171	0.0334	0.0247	0.0377	0.8101
	111	0.0013	0.0158	0.0169	0.0142	0.0290	0.0351	0.8214	0.0467

oracle c

Bernstein-Vazirani Superconductor	0000	0001	0010	0011	0100	0101	0110	0111	1000	1001	1010	1011	1100	1101	1110	1111
0000	0.8350	0.1016	0.0664	0.0127	0.0469	0.0059	0.0127	0.0029	0.0664	0.0098	0.0117	0.0078	0.0166	0.0059	0.0049	0.0029
0001	0.0996	0.7949	0.0107	0.0830	0.0049	0.0420	0.0039	0.0020	0.0059	0.0498	0.0029	0.0029	0.0020	0.0029	0.0010	0.0020
0010	0.0488	0.0137	0.8350	0.0918	0.0049	0.0000	0.0508	0.0059	0.0078	0.0020	0.0596	0.0137	0.0010	0.0010	0.0039	0.0029
0011	0.0059	0.0654	0.0713	0.7988	0.0010	0.0039	0.0088	0.0479	0.0010	0.0059	0.0068	0.0654	0.0000	0.0078	0.0020	0.0068
0100	0.0020	0.0010	0.0010	0.0000	0.7588	0.0898	0.0723	0.0029	0.0000	0.0000	0.0000	0.0000	0.0684	0.1064	0.0059	0.0029
0101	0.0000	0.0049	0.0000	0.0000	0.0967	0.7588	0.0098	0.0654	0.0000	0.0000	0.0000	0.0000	0.0059	0.0020	0.0020	0.0117
0110	0.0010	0.0000	0.0029	0.0000	0.0576	0.0059	0.6904	0.0986	0.0000	0.0000	0.0000	0.0000	0.0068	0.0000	0.0986	0.0156
0111	0.0000	0.0000	0.0010	0.0039	0.0098	0.0732	0.1299	0.7520	0.0000	0.0000	0.0000	0.0020	0.0029	0.0059	0.0107	0.1279
1000	0.0049	0.0020	0.0020	0.0000	0.0010	0.0000	0.0010	0.0000	0.7529	0.1328	0.0830	0.0195	0.0703	0.0137	0.0068	0.0039
1001	0.0000	0.0166	0.0000	0.0000	0.0010	0.0029	0.0000	0.0000	0.0957	0.7178	0.0078	0.0664	0.0020	0.0410	0.0000	0.0029
1010	0.0010	0.0000	0.0098	0.0020	0.0010	0.0010	0.0049	0.0010	0.0586	0.0088	0.7402	0.1270	0.0049	0.0010	0.0381	0.0098
1011	0.0000	0.0000	0.0000	0.0078	0.0000	0.0000	0.0000	0.0039	0.0098	0.0684	0.0840	0.6875	0.0020	0.0029	0.0059	0.0449
1100	0.0020	0.0000	0.0000	0.0000	0.107	0.0029	0.0020	0.0010	0.0010	0.0010	0.0000	0.0000	0.6641	0.1191	0.0615	0.0225
1101	0.0000	0.0000	0.0000	0.0000	0.0049	0.0137	0.0000	0.0000	0.0010	0.0029	0.0010	0.0010	0.0918	0.6221	0.0020	0.0615
1110	0.0000	0.0000	0.0000	0.0000	0.0010	0.0000	0.0117	0.0010	0.0000	0.0000	0.0020	0.0010	0.0566	0.0166	0.6846	0.1240
1111	0.0000	0.0000	0.0000	0.0000	0.0000	0.0000	0.0020	0.0156	0.0000	0.0010	0.0010	0.0059	0.0049	0.0518	0.0723	0.5576

detected
state

oracle c

Bernstein-Vazirani Ion Trap	0000	0001	0010	0011	0100	0101	0110	0111	1000	1001	1010	1011	1100	1101	1110	1111
0000	0.9481	0.0304	0.0446	0.0080	0.0577	0.0087	0.0096	0.0056	0.0390	0.0096	0.0104	0.0095	0.0094	0.0077	0.0081	0.0099
0001	0.0141	0.9093	0.0009	0.0310	0.0016	0.0508	0.0002	0.0023	0.0010	0.0376	0.0003	0.0025	0.0004	0.0033	0.0005	0.0006
0010	0.0116	0.0009	0.8889	0.0259	0.0008	0.0004	0.0319	0.0021	0.0007	0.0005	0.0320	0.0023	0.0002	0.0003	0.0024	0.0010
0011	0.0003	0.0176	0.0201	0.8668	0.0000	0.0010	0.0012	0.0335	0.0000	0.0014	0.0013	0.0425	0.0001	0.0002	0.0001	0.0036
0100	0.0137	0.0006	0.0008	0.0003	0.8781	0.0323	0.0370	0.0074	0.0006	0.0003	0.0001	0.0004	0.0192	0.0025	0.0021	0.0009
0101	0.0001	0.0164	0.0000	0.0009	0.0176	0.8325	0.0013	0.0267	0.0000	0.0006	0.0000	0.0002	0.0006	0.0283	0.0001	0.0020
0110	0.0002	0.0000	0.0184	0.0008	0.0182	0.0028	0.8552	0.0327	0.0000	0.0002	0.0006	0.0002	0.0006	0.0004	0.0279	0.0031
0111	0.0000	0.0008	0.0003	0.0241	0.0005	0.0308	0.0245	0.8235	0.0002	0.0003	0.0001	0.0013	0.0002	0.0016	0.0019	0.0400
1000	0.0111	0.0009	0.0014	0.0005	0.0013	0.0005	0.0003	0.0002	0.9005	0.0335	0.0441	0.0111	0.0474	0.0107	0.0120	0.0085
1001	0.0002	0.0216	0.0000	0.0018	0.0000	0.0016	0.0002	0.0004	0.0208	0.8647	0.0011	0.0302	0.0015	0.0352	0.0002	0.0019
1010	0.0003	0.0000	0.0229	0.0013	0.0000	0.0002	0.0013	0.0003	0.0013	0.0021	0.8517	0.0271	0.0010	0.0004	0.0293	0.0033
1011	0.0000	0.0004	0.0006	0.0370	0.0002	0.0002	0.0003	0.0028	0.0006	0.0230	0.0306	0.8366	0.0002	0.0013	0.0014	0.0322
1100	0.0002	0.0002	0.0000	0.0000	0.0215	0.0024	0.0020	0.0008	0.0174	0.0012	0.0015	0.0007	0.8636	0.0375	0.0402	0.0083
1101	0.0000	0.0001	0.0003	0.0001	0.0008	0.0340	0.0001	0.0024	0.0006	0.0231	0.0002	0.0017	0.0275	0.8365	0.0013	0.0284
1110	0.0000	0.0002	0.0006	0.0001	0.0006	0.0003	0.0334	0.0032	0.0007	0.0004	0.0248	0.0011	0.0266	0.0026	0.8368	0.0387
1111	0.0000	0.0005	0.0003	0.0014	0.0010	0.0016	0.0013	0.0561	0.0003	0.0015	0.0010	0.0324	0.0014	0.0318	0.0358	0.8177

detected
state

oracle s

Hidden shift Superconductor	0000	0001	0010	0011	0100	0101	0110	0111	1000	1001	1010	1011	1100	1101	1110	1111
	0.3604	0.0693	0.1543	0.0352	0.0791	0.0283	0.0508	0.0156	0.0781	0.0234	0.0547	0.0156	0.0518	0.0186	0.0352	0.0068
	0.0674	0.4219	0.0576	0.1416	0.0205	0.0820	0.0146	0.0381	0.0146	0.0947	0.0176	0.0352	0.0225	0.0430	0.0049	0.0371
	0.1367	0.0352	0.3379	0.0752	0.0469	0.0127	0.0742	0.0205	0.0547	0.0137	0.0879	0.0166	0.0381	0.0059	0.0420	0.0156
	0.0361	0.1309	0.0615	0.3799	0.0195	0.0400	0.0176	0.0742	0.0078	0.0313	0.0303	0.0771	0.0146	0.0313	0.0254	0.0566
	0.0693	0.0156	0.0361	0.0146	0.2969	0.0498	0.1475	0.0352	0.0498	0.0088	0.0176	0.0088	0.0586	0.0205	0.0635	0.0176
	0.0117	0.0518	0.0156	0.0303	0.0703	0.3662	0.0313	0.1416	0.0127	0.0518	0.0117	0.0273	0.0225	0.0791	0.0117	0.0205
	0.0479	0.0166	0.0732	0.0254	0.1709	0.0410	0.3271	0.0879	0.0273	0.0078	0.0547	0.0156	0.0576	0.0107	0.0635	0.0176
	0.0117	0.0342	0.0146	0.0518	0.0273	0.1406	0.0654	0.3613	0.0088	0.0313	0.0186	0.0469	0.0088	0.0352	0.0313	0.0791
detected state	0.0771	0.0225	0.0713	0.0107	0.0547	0.0166	0.0313	0.0107	0.3789	0.0664	0.1504	0.0293	0.0713	0.0264	0.0508	0.0117
	0.0195	0.0674	0.0078	0.0381	0.0176	0.0605	0.0117	0.0273	0.0654	0.3955	0.0410	0.1455	0.0254	0.0762	0.0176	0.0371
	0.0488	0.0137	0.0635	0.0283	0.0313	0.0068	0.0410	0.0068	0.1377	0.0410	0.3047	0.0908	0.0410	0.0156	0.0840	0.0303
	0.0117	0.0313	0.0137	0.0830	0.0049	0.0254	0.0176	0.0508	0.0371	0.1172	0.0664	0.3857	0.0146	0.0303	0.0313	0.0791
	0.0449	0.0176	0.0215	0.0098	0.0645	0.0234	0.0674	0.0127	0.0586	0.0107	0.0361	0.0127	0.3076	0.0566	0.1641	0.0361
	0.0166	0.0400	0.0107	0.0186	0.0176	0.0596	0.0127	0.0254	0.0215	0.0674	0.0088	0.0254	0.0547	0.3809	0.0342	0.1436
	0.0273	0.0049	0.0439	0.0146	0.0645	0.0146	0.0771	0.0156	0.0352	0.0117	0.0762	0.0166	0.1787	0.0410	0.2715	0.0693
	0.0127	0.0273	0.0166	0.0430	0.0137	0.0322	0.0127	0.0762	0.0117	0.0273	0.0234	0.0508	0.0322	0.1289	0.0693	0.3418

oracle s

Hidden shift Ion Trap	0000	0001	0010	0011	0100	0101	0110	0111	1000	1001	1010	1011	1100	1101	1110	1111
	0.7730	0.0242	0.0246	0.0082	0.0752	0.0018	0.0023	0.0010	0.0860	0.0032	0.0026	0.0016	0.0210	0.0010	0.0004	0.0017
	0.0236	0.7718	0.0038	0.0312	0.0020	0.0706	0.0002	0.0030	0.0032	0.0916	0.0004	0.0040	0.0006	0.0194	0.0012	0.0022
	0.0226	0.0118	0.7892	0.0246	0.0018	0.0014	0.0790	0.0026	0.0027	0.0008	0.0868	0.0036	0.0010	0.0004	0.0208	0.0028
	0.0200	0.0226	0.0188	0.7690	0.0018	0.0020	0.0023	0.0708	0.0012	0.0028	0.0010	0.0826	0.0012	0.0010	0.0036	0.0182
	0.0716	0.0018	0.0022	0.0014	0.7634	0.0226	0.0220	0.0048	0.0245	0.0010	0.0014	0.0014	0.0550	0.0012	0.0032	0.0020
	0.0018	0.0710	0.0006	0.0030	0.0212	0.7620	0.0043	0.0244	0.0012	0.0270	0.0000	0.0030	0.0016	0.0584	0.0006	0.0035
	0.0034	0.0012	0.0718	0.0022	0.0368	0.0098	0.7847	0.0234	0.0017	0.0002	0.0328	0.0016	0.0046	0.0006	0.0640	0.0040
	0.0012	0.0042	0.0012	0.0682	0.0158	0.0460	0.0213	0.7846	0.0003	0.0016	0.0012	0.0282	0.0026	0.0058	0.0048	0.0702
detected state	0.0546	0.0026	0.0014	0.0012	0.0264	0.0010	0.0008	0.0004	0.7707	0.0268	0.0216	0.0112	0.0408	0.0020	0.0008	0.0013
	0.0022	0.0612	0.0000	0.0042	0.0004	0.0240	0.0003	0.0012	0.7568	0.0268	0.0264	0.0264	0.0016	0.0434	0.0008	0.0033
	0.0024	0.0012	0.0624	0.0026	0.0012	0.0000	0.0257	0.0022	0.0165	0.0064	0.7630	0.0282	0.0020	0.0010	0.0380	0.0027
	0.0014	0.0010	0.0010	0.0604	0.0000	0.0006	0.0003	0.0288	0.0148	0.0206	0.7398	0.0006	0.0006	0.0022	0.0028	0.0418
	0.0194	0.0010	0.0000	0.0004	0.0496	0.0018	0.0020	0.0006	0.0503	0.0012	0.0014	0.0020	0.7716	0.0234	0.0222	0.0108
	0.0010	0.0218	0.0000	0.0026	0.0014	0.0518	0.0000	0.0018	0.0015	0.0556	0.0002	0.0038	0.0274	0.7778	0.0058	0.0308
	0.0014	0.0004	0.0218	0.0014	0.0018	0.0008	0.0518	0.0010	0.0027	0.0008	0.0584	0.0032	0.0468	0.0108	0.8006	0.0362
	0.0004	0.0022	0.0012	0.0194	0.0012	0.0038	0.0028	0.0494	0.0015	0.0036	0.0026	0.0594	0.0216	0.0516	0.0304	0.7685